ARTICLE

Received 00th January 20xx,

Accepted 00th January 20xx

DOI: 10.1039/x0xx00000x

Exploring the interaction between a fluorescent Ag(I)-biscarbene complex and non-canonical DNA structures: a multi-technique investigation

Francesca Binacchi,†*[a] Ester Giorgi,†*[a] Giacomo Salvadori,†*[a] Damiano Cirri,[a] Mariassunta Stifano,[a] Aurora Donati,[a] Linda Garzella,[a] Natalia Busto,[b] Begona Garcia,[c] Alessandro Pratesi,[a] Tarita Biver[a]

Silver compounds are studied mainly as antimicrobial but have anticancer properties, the latter being, in some cases, better than their gold counterparts. In this paper, we analyse the first example of a new Ag(I) biscarbene able to bind non-canonical structures of DNA, more precisely G-quadruplexes (G4) with different signatures depending on the type of G4. Moreover, we show here that this Ag-based carbene binds the i-motif DNA structure. The Au(I) counterpart, investigated for comparison, stabilises mitochondrial G4. Theoretical *in silico* studies evidenced the details for the different binding modes depending on the G4's geometry. The two complexes showed increased cytotoxic activity compared to cisplatin, overcoming its resistance towards ovarian cancer. The binding with other relevant biosubstrates is studied to afford a more complete picture of the possible target of these new drug candidates. In particular, the Ag(I) complex preferentially binds DNA structures over RNA ones, with higher binding constants for the non-canonical nucleic acids with respect to natural calf thymus. As for the possible proteic targets, the interaction with the albumin model protein BSA is also tested.

Introduction

N-heterocyclic carbenes (NHCs) are potent tools demonstrating application both in catalysis and in coordination chemistry with p-block elements and transition metals.[1] The latter opened the use of NHC in the pharmaceutical environment with antimicrobial and anticancer applications. Silver(I) and gold(I) NHC complexes received much interest among the different metal options. Silver compounds are usually studied as antimicrobial agents,[2] but some candidates, like the monocarbene studied by Citta and co-workers, demonstrated promising properties as anticancer drugs surpassing its gold analogue.[3] Another study by Streciwilk and co-workers also indicated the efficacy of an Ag(I)-NHC against Gram-negative bacterial strains.[4] The interest in NHCs started with discovering the antitumor ability of the gold complex auranofin.[5] This drug, originally used to treat rheumatoid arthritis, completed different clinical trials in the United States as an anticancer agent even if, at the moment of this paper, none of the trials continued after phase II and some were withdrawn.[6] The active moiety was found to be the one with the gold metal centre coordinated with the phosphine ligand. This evidence spurred the investigation of several new drugs with modified phosphine ligands.[7,8] Interestingly, the NHC ligands share similar electron donor properties to the phosphine ones and can strongly stabilise their coordination with the metal.[9,10] A review by Aher and colleagues highlights that NHC metal complexes can play a crucial role in treating all types of cancer. All metal complexes considered in this review show good activity, but Au, Pt and Ag make an important contribution and show a surprising cytotoxicity profile compared to cisplatin. Silver complexes demonstrated a great versability of biological action from DNA interactions, mitochondrial membrane depolarisation, ROS production and so on, as described in the review of Raju and colleagues.[11]

However, the various metal-NHCs may have different mechanisms of action. Often, charged metal-NHCs show selectivity for cancer cells, while cisplatin does not show such selectivity.[12] Hence, the research on new pharmaceuticals needs to go beyond the assessment of cellular effects; a thorough analysis of the binding mechanism and some structure-activity relationship (SAR) would enable us to offer drugs with improved profiles. In this frame, the binding to biosubstrates (proteins and nucleic acids) needs to be carefully studied. During these years, the interest in non-canonical DNA

[a] *Department of Chemistry and Industrial Chemistry, University of Pisa, Via G. Moruzzi 13, 56124 Pisa, Italy*
[b] *Departamento de Ciencias de la Salud, Universidad de Burgos, Paseo de los Comendadores s/n, 09001 Burgos, Spain*
[c] *Departamento de Química, Universidad de Burgos, Plaza Misael Bañuelos s/n, 09001 Burgos, Spain*
† These authors contributed equally.
* Corresponding authors: F. Binacchi (francesca.binacchi@dcci.unipi.it), E. Giorgi (ester.giorgi@phd.unipi.it), G. Salvadori (giacomo.salvadori@phd.unipi.it).
Electronic Supplementary Information (ESI) available: NMR spectra, stability and solubility in aqueous solution, cellular tests, BSA interaction, DNA/RNA interaction, G-quadruplexes, experimental details, K summary table. See DOI: 10.1039/x0xx00000x

or RNA structures increased.[13,14] Among them, G-quadruplexes (G4s) and i-motif emerged as promising targets for anticancer drugs.[15,16] The higher presence of these secondary DNA structures in cancerous cells was associated with their involvement in transcription and replication processes, which are known to be overexpressed.[17] Targeting these types of structures may lead to new anticancer drugs with better properties. The metal complexes which are able to bind G4 structures are mainly formed by planar ligands containing a π-delocalized system, which form π stacking interactions with G-quartets.[18] In general, to the best of our knowledge, no silver(I) carbenes able to bind non-canonical structures of DNA are described in the literature. Instead, in the case of gold(I) NHCs, only a few examples are reported. One of the main examples is a caffein-based gold(I) biscarbene, selective for ovarian cancer cells, which is able to selectively bind to and stabilise G4s over DNA double helix due to its planar geometry and for the similarity of the ligand with the guanine base.[15,19] Several molecules have been tested as binders of i-motif structures. However, there was no evidence of selectivity for i-motif structures over other DNA ones.[20,21] Also, metal complexes with terbium or ruthenium were tested and showed low binding affinity and no structure stabilisation.[22–24] The only example of i-motif selectivity over duplex and G4 is a derivative of the antibiotic heliomycin.[25]
Very recently some of these authors have published interesting results on the reactivity of some similar Ag(I) and Au(I) anthracenyl carbenes, demonstrating that they were able to bind nucleic acids but not G4s.[26] Here, anthracenyl complexes with a longer carbon chain on the imidazole were developed, which could both enhance the lipophilicity and act as an arm able to grab the G4 structure.

Results and discussion

Below, first the results of the synthesis and characterisation of $[Ag(BIA)_2]Cl$ are presented together with preliminary experiments that indicate the interesting properties of this metal complex towards cells and common biosubstrates (albumin, natural DNA). Then, the work is extended to unveil the mechanism of interaction focusing on more peculiar polymers (RNAs in single, double and triple helix forms) and non-canonical oligos (i-motif, G-quadruplex).

Synthesis and characterisation

The $[Ag(BIA)_2]Cl$ complex was synthesised following the procedure described in Scheme 1. The synthesis of the ligand BIA (1-(anthracen-9-ylmethyl)-3-butyl-1H-imidazolium chloride, **1**) was carried out by adapting the procedure reported in the literature.[27] The silver biscarbene (**2**) was obtained by mixing **1** with 0.75 eq of Ag_2O in a polar solvent as MeOH for 24 h. We also synthesised the gold biscarbene (**3**), which was obtained by a transmetallation reaction with 1.0 eq of $[AuCl\{S(CH_3)_2\}]$ (Scheme 1). Compounds **2** and **3** were characterised through ^1H, ^{13}C NMR (Figures S1-S7) and CHN analysis. A ^1H-^1H COSY NMR was carried out for **1** to highlight the coupling between H1 and H2 of anthracene, and consequently to assign correctly the signals in the ^1H spectrum (Figure S3).

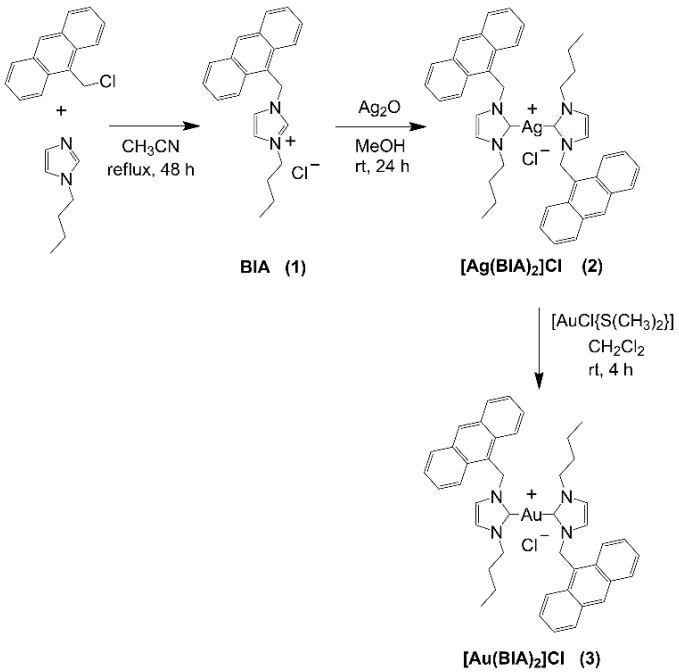

Scheme 1 Synthesis of bis(1-(anthracen-9-ylmethyl)-3-butylimidazol-2-ylidene) silver chloride $[Ag(BIA)_2]Cl$ (**2**), and bis(1-(anthracen-9-ylmethyl)-3-butylimidazol-2-ylidene) gold chloride $[Au(BIA)_2]Cl$ (**3**).

The solubility and stability of the complexes in the buffer solution (NaCl 0.1 M, NaCac 2.5 mM, pH = 7.0) over the time (0-3 h) and in function of the temperature (25-90 °C) were assessed by UV-Vis experiments. The experimental details can be found in the Supporting Information (Figures S8-S11). On the whole, differently from $[Ag(BIA)_2]Cl$ which was stable in the investigated range of temperature and time, $[Au(BIA)_2]Cl$ showed non-negligible stability problems depending on the buffer used, and namely solubility issues due to aggregation phenomena. Therefore, it was impossible to perform a comprehensive study of $[Au(BIA)_2]Cl$ reactivity. However, with due care, a few tests were feasible and provided information to compare the features driven by the two different metal centres. For $[Ag(BIA)_2]^+$, absorbance and fluorescence tests were performed to ensure the direct proportionality between signal and molar concentrations that will be assumed to analyse the data (Figures S12-S14). The same experiments indicated no auto-aggregation of $[Ag(BIA)_2]^+$ when alone in the buffer in the range between 0 and 3.5×10^{-5} M.

Cellular assays

Cytotoxicity. The antiproliferative activity of the silver and gold biscarbenes was investigated on different cancer cell lines. A549 (lung), SW480 (colorectal), and A2780 (ovarian) cells were selected. The comparison with a cell line resistant to cisplatin, i.e. A2780cis, was done to calculate the resistance factor ($RF = IC_{50(A2780cis)}/IC_{50(A2780)}$). The selectivity index (SI) was assessed by comparing the IC_{50} value for A2780 with that

obtained for the healthy cell line, HEK293 (human embryonic kidney). All the values of IC_{50} are summed up in Table 1 where the mean ± standard deviation of three different experiments have been reported and the values compared to that of cisplatin (CDDP), which is still the most used therapeutic agent in cancer therapy. The percentage of surviving cell profiles as a function of $[Ag(BIA)_2]^+$, $[Au(BIA)_2]^+$, and CDDP concentration are reported in Figure S15. Both complexes showed increased cytotoxicity with respect to CDDP with all the selected cancer cell lines, from 4 to 40 times higher, especially in lung cancer. Complex $[Au(BIA)_2]Cl$ turned out the most cytotoxic. It may overall be said that both complexes seem to improve the cellular effects, with $[Ag(BIA)_2]Cl$ being better than $[Au(BIA)_2]Cl$ for both RF and SI.

Table 1 IC_{50} (μM) values of $[Ag(BIA)_2]Cl$ (**2**), $[Au(BIA)_2]Cl$ (**3**) and reference complex cisplatin (CDDP), in cell lines A549 (lung), SW480 (colorectal), A2780 (ovarian), A2780cis (ovarian resistant to cisplatin) and HEK293 (human embryonic kidney) after 24 h of incubation. Mean ± SD from three independent experiments.

	A549	SW480	A2780	A2780cis	RF[a]	HEK293	SI[b]
2	10±2	10±2	6.0±0.4	4.0±0.5	0.7±0.1	15.0±0.2	2.5±0.2
3	1.2±0.1	3.3±0.4	1.0±0.5	1.4±0.5	2±1	2.2±0.9	2±1
CDDP	39±2	35±2	8±1	30±3	4±1	15±2	1.9±0.5

a: RF (resistance factor) = $IC_{50,A2780cis}$ / $IC_{50,A2780}$
b: SI (selectivity index) = $IC_{50,HEK293}$ / $IC_{50,A2780}$

To assess if the cell death mechanism is apoptotic or necrotic, a flow cytometry experiment was performed on A549 cells with Annexin V-FITC/PI double staining (Figure S16). The sum of cells in early and late apoptosis was higher compared to the number of cells in necrosis for both complexes (Figure S17). These values confirm that the cell death mechanism is apoptosis.

Cellular uptake and $logP_{o/w}$. The cellular uptake was tested on the A549 cancer cell line and the obtained values (mean over three experiments) are reported as μmol of metal in 10^6 cells. These data were compared to the lipophilicity of the complexes, which was evaluated by the octanol/water partition coefficient, $logP_{o/w}$ (Table S1). Both compounds exhibit an increased lipophilic character and cellular uptake compared to CDDP. However, $[Au(BIA)_2]Cl$ shows the same uptake level as $[Ag(BIA)_2]Cl$ but is 10 times more cytotoxic. On the whole, lipophilicity alone does not explain the cytotoxicity differences.

Proteins: bovine serum albumin (BSA) interaction

Spectrofluorometric titrations. Serum albumin is the most abundant protein in our blood and albumin binding can be studied to check the possible transport in the bloodstream of the tested drug to reach the tumour site. Bovine serum albumin (BSA) golden standard was selected for these studies. The interaction of $[Ag(BIA)_2]^+$ with BSA was analysed by spectrofluorimetric titrations. BSA has an intrinsic fluorescence at λ_{ex} = 280 nm and maximum emission peaked at λ_{em} = 350 nm. Note that, due to the presence of the anthracenyl moieties and under this excitation, $[Ag(BIA)_2]^+$ emits light with an emission band starting at about 380 nm. Thus, data at λ_{em} > 380 nm were neglected. The titrations were done in buffer (0.1 M NaCl buffer, 2.5 mM NaCac, pH = 7.0) by adding increasing amounts of metal complex to the protein, in triplicate and at different temperatures (from 15.0 to 48.0 °C). An example of titration at 25.0 °C is reported in the Supporting Information (Figure S18). The equilibrium constants for the binding (K_{BSA}) calculated by using the HypSpec® software are collected in Table S2. A 1:1 metal complex to protein binding model was found to be sufficient to reproduce the fluorometric results. It is found that the K_{BSA} value is of the magnitude order of 10^6 (2.9×10^6 M^{-1} at 37.0 °C) and increases by increasing temperature (entropically-driven exothermic process). Given that the thermodynamic signature could be indicative of the type of interaction that occurs between a small molecule and the protein.[28] Here, the positive ΔH value indicates that, for the $[Ag(BIA)_2]^+$/BSA system, hydrophobic interactions are the majority, in agreement with $logP_{o/w}$ = 1 and hinting at a predominant contribution of the anthracenyl residue.[29] To determine which is the BSA preferential (if any) site for the metal complex, a standard procedure was followed which involves performing displacement titrations. First, the protein is saturated with a marker which specifically binds to one of the two BSA binding sites; phenylbutazone (for site I) or ibuprofen (for site II) were selected.[30] Second, displacement experiments were performed by adding increasing amounts of the metal complex to marker+BSA mixtures.

The equilibrium constants related to these displacement titrations (HypSpec® software) are collected in Table S3: a significant decrease of K_{BSA} occurs in the presence of ibuprofen (from 19.2×10^5 M^{-1} to 5.8×10^5 M^{-1}), while the variation is much more limited in the case of phenylbutazone. This suggests that $[Ag(BIA)_2]^+$ and ibuprofen compete for the same site, i.e. the site II.

Mass Spectrometry (MS). The high-resolution ESI-MS analysis, in native conditions, was performed for BSA alone and BSA in the presence of an excess of metal complexes (Figures 1 and S19). For both compounds $[Ag(BIA)_2]^+$ and $[Au(BIA)_2]^+$, the peak of the protein decreases in intensity, in favour of the formation of adducts with the metal complexes. In native conditions, like those preserved in this experiment, serum albumin possesses only one reduced cysteine residue (Cys34) which is solvent exposed.[31] It was extensively reported that this amino acid residue is the preferred binding site for gold-based complexes that covalently interact with the thiolic group.[32,33] Similarly to these findings, it seems reasonable to expect that both complexes interact with the BSA through the loss of one carbene ligand and the subsequent coordination of the metal centre to the sulphur atom of the Cys34 residue.[34–39] The Ag(I) complex forms a single adduct as mono carbene $[Ag(BIA)]^+$ covalently bonded to Cys34 side chain (Figure 1). Moreover, the figure shows three peaks due to the differently metalated BSA adducts. Literature data point at the possibility to form mono and bis adducts of Au(I) complexes on the same

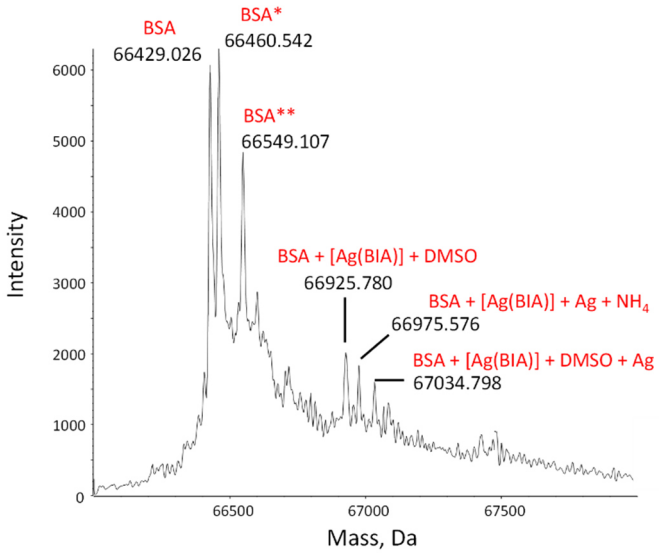

Figure 1 Deconvoluted mass spectra of BSA, C_{BSA} 1.00 µM, in presence of 2.00 µM of $[Ag(BIA)_2]^+$ in NH_4OAc solution 20 mM, pH = 6.8, 0.1% v/v of formic acid has been added just before injection into the mass spectrometer. BSA* = sulfinilation on Cys34; BSA** = cysteinylation on Cys34.[35]

cysteine residue (transient kinetic adduct on Cys34 side chain at short incubation times where two gold metal centres are coordinated to the same sulphur atom)[40]; this behaviour is highlighted also in this case by the signals at 66938 and 67448 Da, respectively (Figure S19B). Note that the protonation state of the protein alone and in the presence of the metal complexes doesn't change, suggesting that the interaction does not cause denaturation of the protein by altering its folding (Figure S20).

On the whole, the binding mode seems two-pronged: at least $[Ag(BIA)_2]^+$ is found to both covalently bind Cys34 and to reversibly enter the site II pocket.

Gel electrophoresis. Native gel electrophoresis was performed to investigate possible conformation changes of the protein upon interaction with the metal complexes. A negative control at different percentages of DMSO confirmed that the employed range was irrelevant. In the presence of $[Ag(BIA)_2]^+$ and $[Au(BIA)_2]^+$ complexes, both didn't cause any conformational change to BSA (Figure S21). The binding mode with the protein does not affect the BSA native conformation, confirming the ESI-MS experiments (Figure S20).

Nucleic acids: natural DNA interaction

Spectro-photometric/fluorometric titrations. During the spectrophotometric titrations, where increasing amounts of natural calf thymus DNA (CT-DNA) are added to the metal complex, the absorbance spectrum of $[Ag(BIA)_2]^+$ showed a dramatic hypochromic effect and a bathochromic shift of 7 nm; also, an isosbestic point appeared at 393 nm (Figure 2A). These results suggest a significant alteration of the electronic levels and represent the first signal of some stacking (groove/intercalative) interaction of the silver complex. As already explained, the gold counterpart suffers from stability problems, but, in the presence of an equal amount of CT-DNA under low ionic strength conditions, the signal is stable. Under these circumstances, the spectrophotometric titration with CT-DNA produces only limited changes in the absorbance profile: first a hypochromic effect, then a hyperchromic bathochromic effect (2 nm, Figure S22A). This dual behaviour is non-rarely found in the case of DNA-interacting systems[41] but here the very slight spectral variations seem related to solubility and aggregation issues only (likely in the polynucleotide grooves).

Since both the complexes bear an anthracenyl fluorophore, we evaluated the DNA interaction also with spectrofluorimetric titrations. The high fluorescence of $[Ag(BIA)_2]^+$ allowed us to use lower concentrations of the complex (0.216 µM), while, for the gold compound the quantum yield was much lower and we used the same conditions of the spectrophotometric titrations. $[Ag(BIA)_2]^+$ emission decreases upon the addition of an increasing amount of DNA (Figure 2B), in agreement with a strong quenching of the anthracenyl moiety and intercalation between base pairs. On the other hand, $[Au(BIA)_2]^+$ confirmed a double behaviour of the emission spectra (Figure S22B) with a first decreasing phase followed by emission increase (with a redshift of 9 nm). Again, aggregation is a possible explanation; on the whole, the metal centre changes the binding mode which seems of outer-

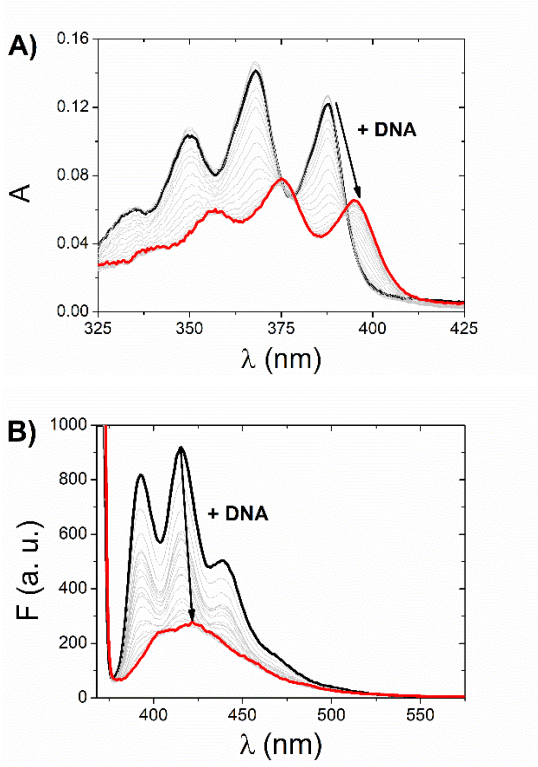

Figure 2 (A) Absorbance spectra corrected for dilution of $[Ag(BIA)_2]^+$ (C_{Ag} = 10.9 µM) at increasing amounts of CT-DNA (C_{DNA}) from 0 (___) to 227 µM (___). (B) Emission spectra (λ_{ex} = 368 nm, slit 5 nm) corrected for dilution of $[Ag(BIA)_2]^+$ (C_{Ag} = 0.216 µM) at increasing amount of DNA from 0 (___) to 59.6 µM (___). NaCac 2.5 mM, pH = 7.0, T = 25.0 °C; C_{DNA} in base pairs.

helix nature and low pharmaceutical significance in the case of the gold compound.[26] Going back to the $[Ag(BIA)_2]^+$/CT-DNA, this system was further investigated by performing absorbance and fluorescence titrations at 25.0 °C and different ionic strength (concentration of NaCl from 0 to 0.1 M, 2.5 mM NaCac buffer). The point is now to apply the best data analysis procedure to obtain a reliable evaluation of the binding constant, K_{DNA}, for these complicated polynucleotide interactions. This system and our data have been used to carry on a critical test on how the numerical evaluations depend on the calculation method employed. This severe issue is frequently underestimated, although the blind application of a non-deeply understood equation may lead to incorrect values. The Scatchard plot[42] was first used to get information on the site dimension of the $[Ag(BIA)_2]^+$/DNA system, i.e. on the number (n) of base pairs involved in the binding of one metal complex (Figure S23). It turns out that n ≈ 1 and thus one base pair is involved. Only once this check was done, it was possible to go ahead considering a simple 1:1 metal complex to DNA base pair reaction and use two equations derived from the Hildebrand-Benesi model[43]

$$\frac{C_P C_D}{\Delta A} + \frac{\Delta A}{(\Delta\varepsilon)^2} = \frac{1}{\Delta\varepsilon}(C_P + C_D) + \frac{1}{K_{DNA}\Delta\varepsilon} \quad (1)$$

$$\frac{\Delta A}{C_D} = \frac{K_{DNA}\Delta\varepsilon[P]}{1 + K_{DNA}[P]} \quad (2)$$

Here, C_i is the total molar concentration of the i-th species, P is the polynucleotide base pair, D is the metal complex, PD is the metal complex/DNA adduct, [P] = C_P – [PD] and [PD] = $\Delta A/\Delta\varepsilon$, $\Delta\varepsilon = \varepsilon_{PD} - \varepsilon_D$ being ε_i the molar extinction coefficient of the i-th species for absorbance (A) mode, K_{DNA} is the equilibrium constant. Given that fluorescence linearity was ascertained, the same equations can be applied to fluorescence data, simply replacing ΔA with ΔF and $\Delta\varepsilon$ with $\Delta\varphi$, being φ the analogous optical factor in fluorescence mode. Note that Eq(1) considers a linear interpolation of the data, while Eq(2) is non-linear. The data analysis went further by using the HypSpec® software on the whole spectral range for n = 1 or even hypothesizing n = 2. Note that n = 2 (two DNA base pairs interacting with one small molecule) corresponds (in the absence of significant site rearrangement statistical effects considered by the McGhee and von Hippel model)[44] to a 1:1 binding but where the DNA concentration is expressed in reaction sites, with C_{DNA}(sites) = C_{DNA}(base pairs)/n. All the values collected are reported in Table S4 and shown in Figure 3.

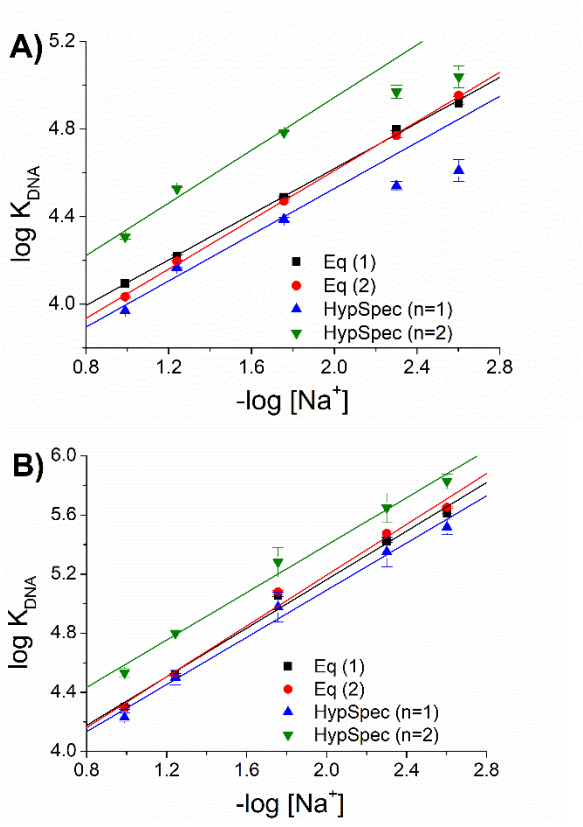

Figure 3 Binding constants (K_{DNA}) for the $[Ag(BIA)_2]^+$/DNA system as a function of the concentration of [Na^+], pH = 7.0, T = 25.0 °C; (A) absorption, (B) fluorescence.

Considering the homogeneous set Eq(1)-Eq(2)-HypSpec(n=1) the agreement was found very good, being the dispersion of data (standard deviation) <1.5% (in log units). Data at -log[Na^+] >2 by the HypSpec analysis were neglected: these were found to suffer some deviation, likely due to DNA-induced aggregation effects. The latter may become more important when using the whole spectral range, at low ionic strength and for the higher concentrations used in the absorbance mode. Note that, interestingly, absorbances or fluorescence experiments return completely different datasets. This behaviour is non-rarely found in the case of DNA when two binding modes are operative. Under these circumstances, K_{DNA} becomes an apparent constant, coming from two contributions that are differently weighted at different experimental conditions. In agreement with the Record theory[45] the slope of the plots shown in Figure 3 corresponds to m'ψ where m' represents the number of phosphodiester residues occupied by a binding molecule and ψ = 0.88 for DNA is a shielding factor. m' also represents the number of sodium ions displaced by a complex molecule and is correlated to the degree of penetration of the small molecule into the helix.[46] The m' values turn to be reproducible, also considering HypSpec(n=2): m' = 0.62±0.04 (ABS), m' = 0.93±0.03 (FLUO). It may be supposed that, in the case of fluorescence, the low concentration conditions repress dye-dye interaction which stabilises groove binding and intercalation is favoured. This picture is confirmed by the higher penetration degree obtained for fluorescence (m' FLUO > m' ABS).

Melting. The melting analysis (Figure S24) unveiled that already when the $C_{[Ag(BIA)2]+}/C_{DNA}$ ratio is equal to 0.5, there is a high stabilization of the double helix (ca. 20 °C, Table S5). Small molecules that interact with the DNA double helix through intercalation can increase the thermal stability by many degrees (commonly > 10 °C); differently, electrostatic interactions and groove binding produce lower variation of T_m.[47] This finding confirms that some intercalation is at play.

Viscosity. The viscosity analysis was carried out by keeping the DNA concentration constant (C_{DNA} = 118 μM) and varying the concentration of the complex to obtain the measurement of viscosity at different $C_{[Ag(BIA)2]+}/C_{DNA}$ ratios (from 0 to 1.0). The relative viscosity (η/η°) does not change much for the $[Ag(BIA)_2]^+$/DNA system (Figure S25). This result could appear in contrast to intercalation that typically involves helix elongation and an increase in viscosity.[48] This experiment confirms that the process is not simple or purely intercalative. Note that in these experiments the concentration of both species is 10-fold higher compared to absorbance titrations (100 μM range). Under these circumstances, DNA-induced aggregation of the complex may compete with the intercalation into the double strand of DNA. It may also be speculated that the anthracenyl residue can undergo some intrastrand crosslinking or may bisintercalate (in the latter case producing a double helix bending that compensates elongation). For gold, the experiment unfortunately suffered precipitation problems.

Gel electrophoresis. Agarose gel electrophoresis tests were done to analyse the interaction between plasmid DNA (pUC18) and the metal complexes (Figure S26). CDDP was used as a positive control for covalent binding (spots 15-16), DMSO as a vehicle negative control (spot 2). Two bands of the plasmid were observed (open circular form (OC) and supercoiled (SC) forms). No changes in the plasmid bands were observed: no covalent binding (as seen for CDDP) and no DNA cleavage occurred.[49] In agreement with previous tests, classical intercalation can be discarded since the migration of the SC band is not affected by the presence of the complexes.[50] The partial intercalation and intrastrand crosslinking option would agree with these findings.

Nucleic acids: RNA interaction

Spectrophotometric titrations and melting tests were repeated with the single-stranded RNA poly(rA), and the double and triple helixes, poly(rA)poly(rU) and poly(rA)2poly(rU). Figure S27 shows the starting spectrum of $[Ag(BIA)_2]^+$ and the final spectra for the $[Ag(BIA)_2]^+$/RNAs mixtures. For all the polynucleotides, no significant signal shifts as those of Figure 2A were observed. In general, in the case of RNAs, the interaction of $[Ag(BIA)_2]^+$ seems impractical and the result is the lack of strong interaction with RNA molecules that can lead to major spectral changes. Melting experiments (Table S6) indicate that there is indeed some interaction between the metal complex and double-stranded RNA, but it is weak (ΔTm of a few degrees from +4.4 to -3.5 °C with the increase of the ionic strength). The silver complex demonstrated a major affinity for DNA double strands over RNA structures.

Non-canonical oligos: i-motif interaction

Spectrophotometric titration and melting. The experiments related to non-canonical oligonucleotides will be discussed in the following sections. Spectrophotometric titrations and melting tests were performed on the $[Ag(BIA)_2]^+$/i-motif (Figure 4). The medium was a buffer solution under acidic conditions (NaCac 50 mM, pH = 5.5), used to preserve the hemi-protonated cytosine-cytosine bond which is fundamental for the existence of the i-motif structure.

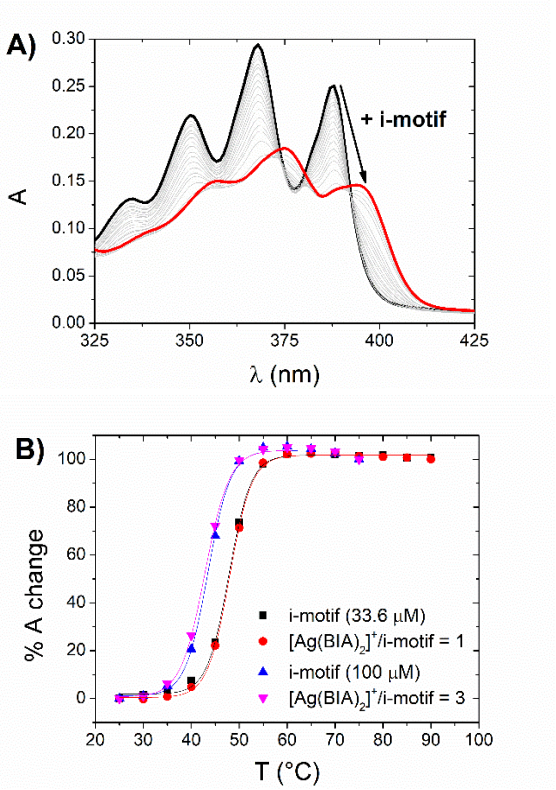

Figure 4 A) Absorbance spectra of $[Ag(BIA)_2]^+$ (corrected by dilution) at increasing amounts of i-motif from 0 to 102 μM (in strands). C_{Ag} = 21.8 μM, NaCac 50 mM, pH = 5.5, T = 25.0 °C. B) Melting curves for i-motif alone (black squares 33.6 μM; blue up triangles 100 μM with 7% of DMSO) and the $[Ag(BIA)_2]^+$/i-motif mixture at $C_{[Ag(BIA)2]+}/C_{i\text{-}motif}$ = 1 (red circles) or 3 (pink down triangles).

These experiment evidence marked hypochromic and bathochromic effects on the silver spectra (similar to what was seen for CT-DNA), that indicate strong i-motif interactions (Figure 4A). On the other hand, there is no significant stabilisation of the $[Ag(BIA)_2]^+$/i-motif adduct (Figure 4B). The latter holds also at higher concentrations of i-motif and silver complex: even at a concentration of the order of 10^{-4} M with a metal complex/i-motif ratio = 3, no stabilisation of the DNA structure was noticed. This behaviour may suggest a type of interaction which involves the groove/external part of the motif. The equilibrium constant was evaluated with the HypSpec® software and a 1:1 binding mode was found to apply. The found value is $K = 3.2 \pm 0.7 \times 10^4$ M^{-1}.

Non-canonical oligos: G-quadruplexes interaction

Spectrophotometric titrations and melting. The behaviour of the $[Ag(BIA)_2]^+$ complex in the presence of three different conformations of G4s (Table 2) was evaluated. All three conformations analysed produce significant hypochromic and bathochromic effects (Figure S28, Table S8), similar to what

happened for CT-DNA (Figure 2A). HypSpec® tests on different reaction models indicate that, in all cases, the formation of a 1:1 adduct metal complex:G4 is sufficient to describe the data. Table 2 collects the obtained numerical values for binding constants.

The G4s melting temperature was measured, in the absence and presence of the metal complex $[Ag(BIA)_2]^+$ (Figure S29).

Table 2 Equilibrium constants from the spectrophotometric titrations for $[Ag(BIA)_2]^+$/G4 systems; KCl 0.1 M, LiCac 2.5 mM, pH 7.0, 25 °C. Melting temperatures (T_m) of G4 alone and $[Ag(BIA)_2]^+$/G4 mixtures. C_{G4} = 25.0 µM (in strands), [complex]/[G4] = 0.5. Here, for c-myc KCl 0.01 M, LiCac 2.5 mM, pH 7.0 (c-myc is very stable and higher KCl content would yield a T_m out of the detection window).

G4	Type	K_{G4} (10^5 M^{-1})	T_m G4 (°C)	T_m $[Ag(BIA)_2]^+$/G4 (°C)	ΔT_m (°C)
Tel-23	Hybrid	18 ± 5	62.8 ± 0.3	63.0 ± 0.3	0.2 ± 0.6
CTA-22	Antiparallel	8.7 ± 0.8	62.6 ± 0.2	66.2 ± 0.3	3.7 ± 0.5
c-myc	Parallel	7.2 ± 0.8	74.0 ± 0.4	78.4 ± 0.3	4.4 ± 0.7

Table 2 collects also these data. Overall, the data seem to suggest that Tel-23 (hybrid G4) behaves differently from CTA-22 (antiparallel G4) and c-myc (parallel G4) which are similar to each other. Although $[Ag(BIA)_2]^+$/Tel-23 is favoured (high K_{G4}, Table 2), the interaction does not produce a stabilization of the quartet which opens as easily as the G4 alone. It may be speculated that the binding site is external to the quartet like in the groove of the G4 structure.[51] Depending on the geometry, the metal complex seems to bind to two different sites: one binding mode affects more the quartet, while the other does not. It was already noticed in the literature that hybrid conformations are less stabilised by the interacting compounds.[51] The situation of CTA-22 and c-myc is the opposite: the interaction is overall slightly less favourable but affects and stabilizes the quartet.

FRET melting. In FRET experiments we used doubly labelled oligonucleotides with two fluorescent probes, one acts as donor, FAM (5(6)-carboxyfluorescein, F), and the other as acceptor, TAMRA (5(6)-carboxytetramethylrhodamine, T) resumed in Table S10. An intramolecular duplex (FdxT) and different conformations of G4 mixed with increasing amounts of silver or gold biscarbenes were analysed (Figures S30, S31 and S32). In this case, we used a different wavelength (516 nm) to plot the melting profile which enabled us to also evaluate the interaction with the gold counterpart. The G4 structures used here can be compared to the ones analysed in direct melting experiments: F21T (hybrid G4) with Tel-23; F21CTAT (antiparallel G4) with CTA-22. For the silver complex, no significant changes in the melting temperature were noticed. For the gold biscarbene, there was a stabilisation of around 10 °C only in the case of the antiparallel form Fmt9438T which is a mitochondrial G4. The stabilisation of this

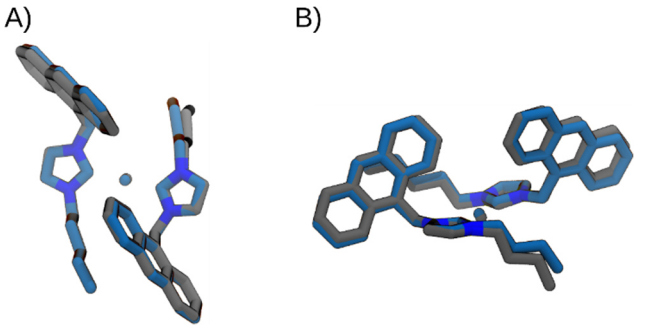

Figure 5 Superimposition of the optimized structures of $[Ag(BIA)_2]^+$, in grey, and $[Au(BIA)_2]^+$, in blue, in two different views: frontal (A) and lateral (B).

G4 is of particular interest since gold complexes are accounted to act in the mitochondria. The stabilisation of four degrees which was determined in the melting test with CTA-22 was not found here with F21CTAT. We may speculate that this may be caused by the fact that in FRET experiments we have not only the G4 but also the fluorophores that could interact with the complexes or hinder their interaction.

In silico studies - PCM. In solution, the structures of the Au(I) and Ag(I) complexes are comparable (Figure 5). However, a different degree of distortion can be highlighted, and it cannot be excluded that the latter could produce consequences in the interaction with biomolecules. Indeed, the carbon-metal distances are equal to 2.047 Å and 2.104 Å, respectively. Both structures show a slight deviation in linearity with respect to the C-Ag/Au-C bond angle (175° and 172° for the Au(I) and Ag(I) complexes, respectively). Relaxed scans of the NHC-NHC dihedral angles were performed for both the cationic complexes to investigate the energetic barrier of the rotation of the NHC rings (Figure S33).

The energetic profile is very similar for both complexes. The main differences can be attributed to the equilibrium value (-9° and -7°, for Ag and Au complexes, respectively), and to the torsional barrier, which is slightly lower in the $[Ag(BIA)_2]^+$ complex.

In silico studies - Molecular docking. Before performing molecular docking calculations, each G4 was subjected to a 1.5 µs-long molecular dynamics simulation to incorporate receptor flexibility through ensemble docking.[52–54] We computed the RMSD on the heavy atoms of each G4, backbone, and guanine residues (Figure S34). This shows a stable structure after 500 ns, except for a peak in CTA-22 due to a temporary opening of the terminal part of the nucleic acid. From each ensemble, we randomly sampled 50 structures for the next docking procedure. The sampling has been performed taking into account only the last 1 µs. The lowest docking binding energies of the Au(I)/Ag(I) complexes with G4 targets are shown in Table S7.

The docked models (Figure 6) suggest that for $[Au(BIA)_2]^+$ complex in c-myc a more stable groove binding mode is predicted. For what concerns $[Ag(BIA)_2]^+$, we identified a stacking interaction to the thymine residue of the loop regarding c-myc and CTA-22. Specifically, the interaction occurs with one thymine of c-myc and one of CTA-22 marked

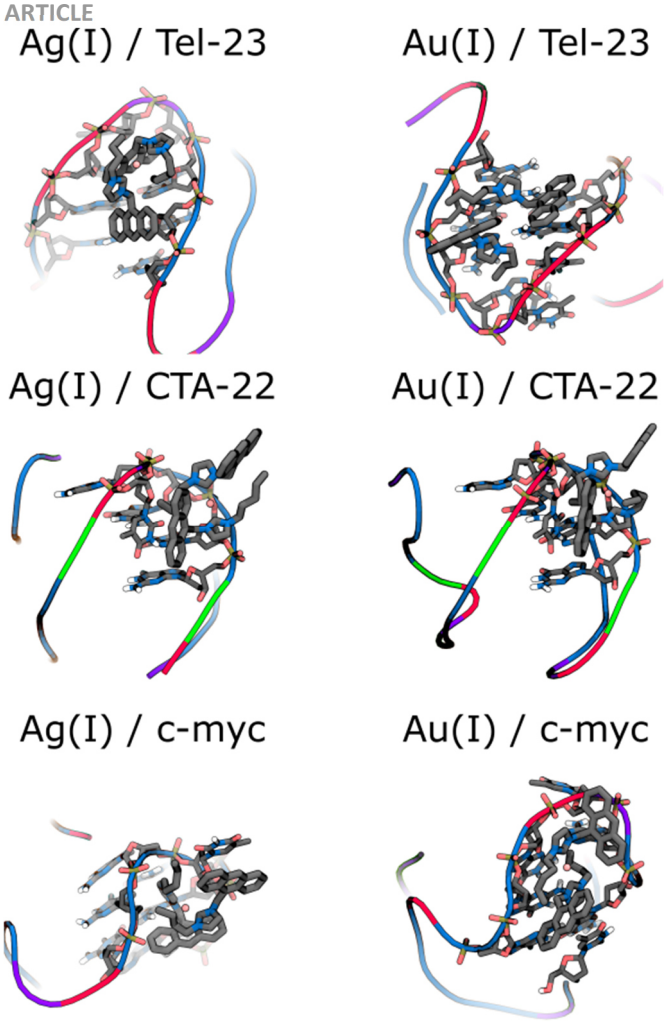

Figure 6 Most stable binding poses for the two ligands in G4s. Adenine, guanine, cytosine, and thymine residues are coloured in violet, blue, green, and red, respectively. Residues within 4 Å from the complex are shown.

bold in the sequences: 5'-TGAGGG**T**GGGTAGGGTGGGTAA-3', 5'-AGGGCTAGGGC**T**AGGGCTAGGG-3' respectively. The same interaction occurs for $[Au(BIA)_2]^+$ with CTA-22.

Regarding the interaction between c-myc and $[Ag(BIA)_2]^+$, can also be observed an additional intramolecular interaction between the anthracene and the central ring, which contributes to the decrease in the scoring value. There are cases with a major contribution of one of the carbene ligands with the other one facing outwards. Even in these cases the presence of the second ligand may be supposed to play a role considering that the overall metal complex: (i) will become positively charged, a feature that can drive the binding mode;[55] (ii) will acquire a given geometrical form, again important for pushing more favourable binding matches at the different oligos.

Finally, both complexes show a groove interaction in Tel-23, as the most stable binding modes. In particular, the silver complex interacts with the sugar of the thymine and guanine residues marked bold: 5'-TAGGGTTAGGG**T**TAG**G**GTTAGGG-3'.

Experimental

Metal complexes. Stock solutions of the metal complexes were prepared by dissolving a known weighted amount of the compound (≈ 2 mg) in dimethylsulfoxide (DMSO) to obtain a final solution concentration of 2 - 20 mM. Stock solution of cisplatin (CDDP) was prepared in water to obtain a final concentration of 3 mM.

Biosubstrates. The BSA solution was prepared by weighing freeze-dried BSA purchased from Sigma-Aldrich (MW ≈ 66 kDa) (lyophilized powder, essentially fatty acid-free, ≥98% (agarose gel electrophoresis) by dissolving it in NaCl 0.1 M, NaCac 2.5 mM, pH = 7.0 buffer. The effective concentration was determined by spectrophotometry (λ = 278 nm, ε = 45000 $cm^{-1}M^{-1}$)[56] obtaining a solution of BSA (C_{BSA}) 80 µM. Calf thymus DNA (CT-DNA), natural DNA from calf thymus, lyophilised sodium salt from Sigma-Aldrich (double strand in the B-helix form when in the buffer) was dissolved in ultrapure water and previously sonicated to have about 500 base pairs. Its concentration in the stock was about 2.5 mM expressed in base pairs (C_{DNA}). Before its use, the exact concentration value was checked by acquiring an absorption spectrum (λ = 260 nm, ε = 13200 $cm^{-1}M^{-1}$).[57]

Cell lines and *E. coli* DH5α were purchased from ATCC.

Natural DNA, the plasmid pUC18 (2686 base pairs in length) was extracted from *E. coli* DH5α and purified by a HP Plasmid Midi kit (Omega Biotek, VWR). The plasmid was used to perform agarose gel electrophoresis experiments.

Poly(rA) and poly(rU) were purchased by Sigma-Aldrich as model polynucleotides of RNA structures. Poly(rA) was used as a single filament in NaCac 2.5 mM pH = 7.0 buffer, whose concentration was measured by spectrophotometry (λ = 257 nm, ε = 10110 $cm^{-1}M^{-1}$)[58] obtaining a concentration expressed as phosphate groups (C_A) of 8.4 mM. For the double helix, a poly(rU) solution was prepared in the same buffer whose concentration was measured considering the peak at 260 nm (ε = 8900 $cm^{-1}M^{-1}$)[58] obtaining a concentration value of 14 mM. A solution of poly(rA) with poly(rU) in a 1:1 ratio in buffer was then prepared and left to stand overnight in the dark at room temperature to obtain the double helix poly(rA)poly(rU) concentration in base pairs (C_{AU}) 2.0 mM. For the triple helix, a solution was prepared by combining poly(rA)·poly(rU) with poly(rU) in a 1: 1 ratio in buffer and left to stand overnight at room temperature to allow the integration of a third filament in the structure, thus obtaining a solution of poly(rA)2poly(rU) of concentration in base triplet (C_{A2U}) 0.4 mM.[59]

The i-motif used was obtained by dissolving the $(CCCTTT)_4$ telomere in NaCac 50 mM, pH = 5.5 buffer solution in a concentration of 1 mM. The procedure for the annealing it's the same as described below for G4.

The DNA G-quadruplexes (G4) used were formed by different telomeres to have different types of conformations: 5'-TAGGGTTAGGGTTAGGGTTAGGG-3' (Tel-23 – hybrid); 5'-AGGGCTAGGGCTAGGGCTAGGG-3' (CTA-22 – antiparallel); 5'-TGAGGGTGGGTAGGGTGGGTAA-3' (c-myc – parallel) were dissolved in KCl 0.1 mM, LiCac 2.5 mM, pH = 7.0 obtaining a

solution of G4 (C_{G4}) 1 mM. The telomere annealing procedure to form the quaternary structure consists of placing the Eppendorf tube which contains the telomere solution in a thermostatic water bath by slowly heating from a temperature equal to that of the environment up to about 90-95 °C. The maximum temperature was maintained for 10-15 min and then the heating was turned off and the solution was allowed to cool slowly in the water bath until the next morning.[60]

Buffers. The used buffer solutions were prepared by dissolving a known amount of the desired salts in MilliQ water, obtained through an "AriumPro SARTORIUS" device, and the pH was possibly corrected by making micro additions of HCl or concentrated NaOH. The salts used to prepare buffer solutions were sodium chloride (NaCl), sodium cacodylate (NaCac, caution: cacodylate is toxic if swallowed or inhaled) potassium chloride (KCl), lithium cacodylate (LiCac), ammonium acetate (NH_4OAc). Working solutions are prepared by dilution of the metal complex or biosubstrates in the correct buffer so that DMSO content can be considered negligible (< 1%).

Synthesis of BIA (1). 453 mg of 9-chloromethylantracene and 248 mg of 1-butylimidazole were dissolved in 40 mL of acetonitrile. The reaction was stirred for 46 hours at 80 °C. The solvent was then evaporated under reduced pressure and a yellow solid was obtained. The latter was dissolved in a few millilitres of methanol, then diethyl ether was slowly added to precipitate the final product, which was obtained as a fine yellow powder. (Yield 85%) ^{1}H-NMR ($CDCl_3$, 400 MHz) δ = 11.18 (s, 1H, imidazole H2'), 8.49 (s, 1H, anthracene H10), 8.30 (d, 2H, anthracene H1 and H8, J = 8,8 Hz), 7.99 (d, 2H, anthracene H4 and H5, J = 8,4 Hz), 7.60-7.56 (m, 2H, anthracene H2 and H7), 7.47-7.43 (m, 2H, anthracene H3 and H6), 7.18 (m, 1H, imidazole H4'), 6.64 (m, 1H, imidazole H5'), 6.60 (s, 2H, anthracene-C**H$_2$**-imidazole), 4.23 (t, 2H, imidazole-C**H**$_2$CH$_2$CH$_2$CH$_3$, J=7.6 Hz), 1.86-1.79 (m, 2H, imidazole-CH$_2$C**H**$_2$CH$_2$CH$_3$), 1.34-1.25 (m, 2H, imidazole-CH$_2$CH$_2$C**H$_2$**CH$_3$), 0.87 (t, 3H, imidazole-CH$_2$CH$_2$CH$_2$C**H$_3$**, J=7.2 Hz) ppm. ^{13}C ($CDCl_3$, 400 MHz) δ =137.75, 131.33, 130.94, 130.62, 129.59, 128.36, 125.62, 122.85, 122.10, 121.64, 121.07, 50.04, 45.61, 32.09, 19.53, 13.46 ppm.

Synthesis of [Ag(BIA)$_2$]Cl (2). 527 mg of ligand BIA (**1**) were dissolved in 8 mL of methanol in a 50 mL flask, with 263 mg (0.750 eq) silver oxide Ag_2O. The mixture was stirred at room temperature for 24 hours. Then dichloromethane was added, and the suspension was filtered through celite to remove the unreacted Ag_2O and the eventual unreacted ligand. The solvent was removed under reduced pressure, obtaining a red amorphous solid. Subsequently, the solid was dissolved in 8 mL of methanol and the solution was kept stirring at room temperature for 24 hours, protected from the light. After this time, the suspension was filtered through celite to remove AgCl. The solvent was evaporated, and crystallisation was carried out using THF/Et_2O. The light orange granular solid was filtered and washed with hexane. (Yield 12%) ^{1}H-NMR (CD_3OD, 400 MHz) δ = 8.56 (s, 2H, anthracene H10), 8.14 (d, 4H, anthracene H1 and H8, J = 7.2 Hz), 8.04 (d, 4H, anthracene H4 and H5, J = 6.8 Hz), 7.53-7.44 (m, 8H, anthracene H2,3,6,7), 7.30 (s, 2H, imidazole H4'), 7. 19 (s, 2H, imidazole H5'), 5.90 (s, 4H, anthracene-CH$_2$-imidazole), 3.47 (b, 4H, imidazole-C**H**$_2$CH$_2$CH$_2$CH$_3$), 1.71 (b, 4H imidazole-CH$_2$C**H**$_2$CH$_2$CH$_3$), 1.20 (b, 4H imidazole-CH$_2$CH$_2$C**H**$_2$CH$_3$), 0.89 (b, 6H imidazole-CH$_2$CH$_2$CH$_2$C**H**$_3$) ppm. ^{13}C (CD_3OD, 400 MHz) δ = 170.27, 133.02, 132.11, 130.62, 128.45, 127.04, 126.45, 124.60, 123.69, 123.40, 121.98, 53.09, 47.76, 34.41, 20.28, 13.74 ppm. Elemental C, N and H analysis of $C_{44}H_{44}N_4AgCl$: calculated C = 68.44%, H = 5.74%, N = 7.26% and experimental C = 68.24%, H = 5.62%, N = 6.89%.

Synthesis of [Au(BIA)$_2$]Cl (3). To synthesise the [Au(BIA)$_2$]Cl complex, the transmetalation of [Ag(BIA)$_2$]Cl was carried out, using [AuCl{S(CH$_3$)$_2$}]. To 38.0 mg of [Ag(BIA)$_2$]Cl, 5 mL of CH_2Cl_2 and 15.6 mg (1.00 eq) of [AuCl{S(CH$_3$)$_2$}] were added. The mixture was left stirring at room temperature for 3 hours, protected from the light. The suspension was then filtered over Celite to remove the AgCl formed, and the filtrate was concentrated under vacuum. Precipitation of the metal complex was carried out using hexane. (Yield 87%) ^{1}H-NMR (CD_3OD, 400 MHz) δ = 8.57 (s, 2H, anthracene H10), 8.28 (d, 4H, anthracene H1 and H8, J = 7.2 Hz), 8.05 (d, 4H, anthracene H4 and H5, J = 6.8 Hz), 7.56-7.46 (m, 8H, anthracene H2,3,6,7), 7.21 (s, 2H, imidazole H4'), 7.06 (s, 2H, imidazole H5'), 6.07 (s, 4H, anthracene-CH$_2$-imidazole), 3.80 (m, 4H imidazole-C**H**$_2$CH$_2$CH$_2$CH$_3$), 1.67-1.59 (m, 4H imidazole-CH$_2$C**H**$_2$CH$_2$CH$_3$), 1.181-1.088 (m, 4H imidazole-CH$_2$CH$_2$C**H**$_2$CH$_3$), 0.78-0.74 (m, 6H imidazole-CH$_2$CH$_2$CH$_2$C**H**$_3$) ppm. ^{13}C (CD_3OD, 400 MHz) δ = 182.74,131.49, 130.81, 129.30, 129.09, 126.90, 125.11, 124.93, 123.06, 121.16, 121.09, 50.94, 46.25, 32.87, 19.11, 12.37 ppm. Elemental C, N and H analysis of $C_{44}H_{44}N_4AuCl$: calculated C = 61.22%, H = 5.37%, N = 6.49% and experimental C = 61.33%, H = 5.25%, N = 6.16%.

Cell culture. A549 (lung adenocarcinoma) and SW480 (colon adenocarcinoma) cells were cultured in Dulbecco's Modified Eagle's Medium (DMEM), whereas A2780 (ovarian carcinoma) and A2789cis (ovarian carcinoma cisplatin-resistant) cells in Roswell Park Memorial Institute (RPMI) 1640 medium supplemented with 2 mM L-glutamine, and HEK293 (embryonic kidney) cells in Eagle's Minimum Essential Medium (EMEM) supplemented with 1% of non-essential amino acids. All media were supplemented with 10% fetal bovine serum (FBS), fundamental for cell growth, and 1% amphotericin-penicillin-streptomycin solution (all from Sigma Aldrich). Cells are incubated in a humid atmosphere at 37 °C under a 5% CO_2 atmosphere.

MTT assay. Approximately 5×10^3 A549, 1×10^4 SW480, 2×10^4 A2780, A2780cis and HEK293 cells per well were seeded in 200 µL of their culture medium in 96-well plates and incubated for 24 h at 37 °C under a 5% CO_2 atmosphere. Then, the cells were treated with different concentrations of the complexes under study for 24 h. Cisplatin (CDDP) was used as a positive control and the max percentage of DMSO as vehicle control. Dilution of the stock solutions was done in the corresponding culture medium. Negative control (without any treatment) and blanks were also included. Afterwards, the medium was removed, and cells were incubated with 100 µL of MTT (3-(4,5-

dimethyltiazol-2-yl)-2,5-diphenyltetrazoliumbromide) (Sigma Aldrich) dissolved in culture medium (500 mg/mL). The reduction of the yellow salt, thanks to mitochondrial dehydrogenase, forms the blue formazan in the living cells. After 3 h of incubation, the formazan crystals were dissolved by overnight incubation with 100 µL of the solubilizing solution (10% SDS and 0.01 M HCl). Finally, the absorbance was read at 590 nm on a microplate reader (Cytation 5 Cell Imaging Multi-Mode Reader, Biotek Instruments, USA). Four replicates per dose were included and at least three independent experiments were performed for the calculation of the half-maximal inhibitory concentration (IC_{50}) values employing GraphPadPrism Software Inc. (version 6.01) (USA).

Apoptosis. was evaluated by flow cytometry with an Annexin V-FITC Assay Kit (Biorad) according to the manufacturer's instructions. 2×10^5 A549 cells were seeded in 1 mL of cell culture medium in 12 well plates. After 24 h of incubation, the cells were treated with the half-maximal inhibitory concentration of each complex for 24 h. Cisplatin (CDDP) was used as positive apoptotic control, while TRITON 1% was used as death (necrotic) control and added 10 minutes before the harvesting of the cells. Afterwards, the cells were washed with cold PBS, harvested, and resuspended in a binding buffer. Then, the cells were doubly stained with the Annexin V-FITC conjugate and propidium iodide (PI). Immediately after PI addition, the cells were injected in a NovoCyte Flow cytometer (ACEA Biosciences, Inc., USA). 10000 events were counted and analysed by using the NovoExpress 1.4.0 Software. Two independent experiments were performed.

Cellular uptake. 1.5×10^5 A549 cells were seeded in 2 mL of cell culture medium in 6 well plates for 24 h. Afterwards, the cells were treated with a concentration of 5 µM for each metal complex for 24 h. CDDP was used as a positive and reference control. The cells were then harvested and washed twice with PBS to remove the metal complex that was not internalised to obtain the cellular pellet. The cells were resuspended in 500 µL of PBS and 10 µL were used to count cells in an automated cell counter (TC-20, BioRad). 2 mL of a solution of HNO_3 Suprapure (dilution 1:1 with MilliQ water) for Ag and Au complexes, or 2 mL of 3HCl : HNO_3 (*aqua regia*) Suprapure solution (dilution 1:1 with MilliQ water) for the Pt complex were added to mineralise the samples (90 °C overnight). A dilution with MilliQ water to have a final volume of 6 mL per sample was done, and ICP-OES analysis was performed as already described.[61,62] The amount of metal internalised by the is expressed in µmol of metal/10^6 cells.

Log$P_{o/w}$. The octanol-water partition coefficients were determined as follows. Water (500 mL, distilled after MilliQ purification) and n-octanol (500 mL) were shaken together for 72 h to allow saturation of both phases (one week for the full separation of the two phases). Approximately 0.5 mg of the complexes were placed into a Falcon tube, and 2 mL of octanol-saturated water and 2 mL of water-saturated octanol were added into the same Falcon of the compound and shacked until the complexes were fully dissolved and divided into the two phases. Biphasic solutions were mixed for ten minutes and then centrifuged for five minutes at 6000 rpm to allow separation. Two aliquots of 500 µL for both phases were placed into metal-free PE tubes and 4 mL of a solution of HNO_3 Suprapure (dilution 1:1 with MilliQ water) for Ag and Au complexes, or 4 mL of 3HCl : HNO_3 (*aqua regia*) solution Suprapure (dilution 1:1 with MilliQ water) for CDDP, were added to the aliquots to obtain 4 samples for each complex (2 for the water phase and 2 for the octanol phase). The solutions were mineralised at 90 °C overnight and 1.5 mL of MilliQ water were added at the end to have a final volume of 6 mL for each sample. The metal concentration in both phases was determined by ICP-OES.[61,62]

Titrations. A *Shimadzu UV-2450* or a *Perkin Elmer Lambda 35* double-beam UV-vis spectrophotometer were used for absorbance experiments. Both instruments are equipped with a tungsten lamp for visible light and a deuterium lamp for the UV range. The fluorescence data were recorded with an *LS55 Perkin-Elmer* spectrofluorometer. The excitation light is provided by a pulsed Xenon lamp (50 Hz). In the spectrophotometric titrations a solution of the metal complex (D) of around 20 µM (C_D), was put in a 1 cm pathway cuvette. After measuring the spectrum of the metal complex alone, increasing amounts of the biosubstrate (P) were added directly to the cuvette containing the metal complex solution and a spectrum was recorded upon each addition. The titration was followed by plotting the binding isotherm (y-axis: $\Delta A/C_D$ where $\Delta A = A - C_D\varepsilon_D$, and ε_D is the molar absorption coefficient of the metal complex; x-axis: C_P). Once the binding isotherm reaches the plateau, the titration is concluded. All the spectra shown are corrected for dilution factors. Fluorescent titrations follow the changes in emission of the fluorescent species upon increasing addition of the quencher. The procedure is similar to the one described for absorbance experiments, where instead of ΔA, there is $\Delta F = F - C_D\phi_D$, and ϕ_D is a proportional constant similar to ε. The data are finally treated with the appropriate equations or software to obtain the desired thermodynamic parameters. The HypSpec® software (www.hyperquand.co.uk) enables the simultaneous fit over a range of wavelengths through a least squares procedure and according to different models of multiple equilibria. Three replicates for each titration were done.

Mass Spectrometry. For the mass spectrometry measurements, all samples were prepared in LC-MS grade solvents or solutions. The high-resolution ESI mass spectra were recorded using an AB SCIEX Triple TOF 5600+ (Sciex, Framingham, MA, USA), equipped with a DuoSpray® interface operating with an ESI probe. All the ESI mass spectra were acquired through a direct injection at 5 µL min^{-1} flow rate. The BSA solutions for mass spectrometry experiments were prepared in NH_4OAc 20 mM, pH = 7.0 and finally diluted in LC-MS grade H_2O containing 0.1% v/v of formic acid (FoA) obtaining a BSA concentration of approximately 0.5 µM. Solutions of BSA containing the metal complexes studied were similarly prepared in various concentration ratios from 1:1 to metal complex excess 3:1, incubated at 10 µM for 4 h at 37.0 °C. The ESI source parameters were optimized as follows for proteins:

positive polarity, ion spray voltage floating 5500 V, temperature 25 °C, ion source gas 1 (GS1) 45 L/min; ion source gas 2 (GS2) 0 L/min; curtain gas (CUR) 12 L/min, declustering potential (DP) 150 V, collision energy (CE) 10 V; acquisition range 1000-2600 *m/z*. For acquisition, Analyst TF software 1.7.1 (Sciex) is used and deconvoluted spectra were obtained by using the Bio Tool Kit micro-application v.2.2 embedded in PeakView™ software v.2.2 (Sciex).

Native PAGE gel electrophoresis. Native polyacrylamide gel electrophoresis (PAGE) tests were performed by incubating BSA (3 µM) overnight with different concentrations of metal complexes for [complex]/[protein] concentration ratios of 5, 10 and 20 in NaCl 0.1 M, NaCac 2.5 mM buffer pH = 7.0 and T = 37.0 °C. Vehicle-treated BSA samples were included as a negative control with the different percentages of DMSO used. After that, 6 µL of sample buffer 2X (0.01% bromophenol blue and 20% glycerol in Tris HCl buffer 0.5 M, pH = 6.8) were added to 6 µL of the sample solutions (final C_{BSA} = 1.5 µM) and loaded onto 10% polyacrylamide gels. Before the loading of the samples, a pre-run was done at 200 V for 1 h, to remove any possible impurity from the gel. Gels were run in native PAGE buffer 250 mM Tris Base, 1.92 M glycine, pH = 8.3 at 6.6 V/cm for 4 h at 4 °C to avoid denaturation of the protein. Finally, gels were stained with Coomassie Brilliant Blue R-250.

Melting. The thermal denaturation process was followed by spectrophotometry with the *Shimadzu UV-2450* spectrophotometer using a Peltier thermostat. Melting experiments were performed in triplicate following the absorbance changes (260 nm for CT-DNA and RNA structures, 290 nm for G4 and i-motif) at increasing temperatures ranging from 25 °C to 90 °C (no incubation time). The scan rate is +5 °C/min every 7.5 minutes, and the solution stays at the current temperature for 5 min before the spectrum is recorded (1.5 min for the recording). To reach the following temperature 1 min is needed. Parameters on the thermostat: Star T = 25 °C; Hold time = 360 s; Speed T = 5 °C; Next T = 37 °C; Pre control = 390 s; Repeat time = 14. Cuvettes of 1.0 cm, 2.0 mm or 1.0 mm light path were used depending on the experiment. A short light path was needed in particular for the oligos (DNA G4s and i-motif) melting tests. The percentage of absorbance change (%A change = 100 × (A(T) – A°)/(A∞ – A°), where A(T) is the absorbance read at each temperature T (°C), A° the absorbance corresponding to the initial plateau and A∞ the absorbance for the final plateau), was plotted against temperature. In this way, a sigmoidal curve is obtained according to Equation 3.

$$\%\, A\ change = \frac{A_T - A_0}{A_\infty - A_0} \times 100 \qquad (3)$$

The melting temperature (T_m) was derived as the maximum of the first derivative of the sigmoidal curve. The concentration of the polynucleotide is around 20 µM and the metal complex is put in an equal amount for the first experiment. If the stabilisation is too high, lower complex concentrations could be investigated. All the experiments were performed by modulating the optimal ionic strength conditions so that the melting temperature of the polynucleotide alone is around 50-60 °C. These conditions allow the appreciation of possible enhancement of T_m. Relevant reference melting temperatures are resumed in Table S9.

Viscosity. The viscometer used is a semi-micro type "Cannon-Ubbelohde" capillary viscometer. To carry out the measurement, 3.0 mL of buffer solution (NaCl 0.1 M, NaCac 2.5 mM, pH = 7.0) volume was taken with a glass pipette and inserted into the viscosimeter. This ends up in the lower tank. The viscometer was placed in a water bath at a constant temperature of 25.0 ± 0.1 °C and left to rest for 15 minutes to allow the solution to reach the desired temperature. The solution was sucked up with a small rubber pump until the liquid almost reaches the exit. After that, DNA was added with a micro-syringe Hamilton connected to a Mitutoyo micrometric screw (the same as the spectroscopic titrations) to have a C_{DNA} = 118 µM and the solution is mixed by pushing up and down the liquid. Every addition of the tested compound was made in the same way as the addition of DNA, like a titration (no incubation time). The flow time is measured with a digital stopwatch. The operation must be carried out for the solvent used (measuring t_{solv}), for the solvent + DNA (t_{DNA}) mixture and for different solvent + DNA + molecule mixtures (t_{sample}). The flow times were measured at least six times and the average flow time was considered. After each use, a washing cycle must be carried out: water - acetone - water - ethanol - N_2. The relative viscosity of the polynucleotide was calculated as follows (Equation 4).

$$\frac{\eta}{\eta^\circ} = \frac{t_{sample} - t_{solv}}{t_{DNA} - t_{solv}} \qquad (4)$$

The relative viscosity is connected to the polynucleotide elongation by $L/L^0 = (\eta/\eta^0)^{1/3}$ where *L* is the length of the bound polynucleotide and L^0 is the length of the free one.

Agarose gel electrophoresis. Agarose gel electrophoresis of pUC18 was performed after overnight incubation at 37.0 °C of the plasmid (6.52 µM, base pairs) in the presence of different increasing concentrations of the tested metal complex or cisplatin in buffer (NaCl 0.1 M, NaCac 2.5 mM, pH = 7.0). A vehicle-treated pUC18 sample was included with the maximum DMSO concentration used in the electrophoresis experiment. After 24 h of incubation at 37.0 °C, loading buffer (4 µL) was added to each sample (20 µL) before being loaded onto 1% agarose gel. Electrophoresis was run at 6.5 V/cm for 130 min. After the run, the gel was stained with a solution of ethidium bromide 1 µg/mL in TAE 1× (buffer solution containing a mixture of Tris base, acetic acid and EDTA) for 1 h. Finally, the gel was visualized by exposure to UV light (312 nm) by a Gel Doc XR + Imaging System (Bio-Rad).

FRET melting. FRET melting assay was performed in a real-time polymerase chain reaction (7500 Fast Real-Time PCR, Applied Biosystems) with the oligonucleotides described in Table S10. Here, the melting of the oligonucleotide is followed by the increase in fluorescence of FAM at the increase in temperature. The sigmoidal fit of normalised FAM fluorescence against temperature provides the melting

temperature as the inflexion point of the curve. DMSO and meso-tetrakis(N-methyl-4-pyridyl)porphyrin ($TMPyP_4$) were used respectively for vehicle and positive control experiments. Stock solutions of the oligonucleotides in 10 mM KCl, 90 mM LiCl, 10 mM LiCac were heated up to 92 °C, kept at that temperature for 6 minutes, and cooled by immediately immersing them in ice, to perform annealing just before the experiment. 12×8-well optical tube strips were filled with 25 µL each (20 µL oligonucleotide + 5 µL metal complex) providing a final oligonucleotide concentration of 0.2 µM, the metal complex concentration of 0.2, 1.0, 2.0 and 4.0 µM (C_D/C_P = 1, 5, 10, and 20), and for the positive control $TMPyP_4$ concentration of 2.0 µM (C_D/C_P = 10). The samples were heated from 25 °C up to 95 °C at 1 °C/min rate. FAM fluorescence intensity (λ_{exc} = 492 nm, λ_{em} = 516 nm) was recorded every 0.4 °C. The experiments were performed in 10 mM KCl, 90 mM LiCl, 10 mM LiCac with no incubation time. The difference between the mid-transition temperature of the oligonucleotide with and without the drug (ΔT_m) was calculated.

***In silico* studies PCM calculations.** The initial structures of the Ag(I) and Au(I) complexes were optimized in water as an implicit solvent at ωb97XD/Def2TZVP level of theory as suggested in previous benchmark works.[63,64] The polarizable continuum model (PCM) was used to account for long-range solvation effects.[65–67] All the calculations were carried out with Gaussian16 software.

Targets set up. The target DNA G-Quadruplex structures (G4s), i.e., Tel-23, CTA-22, and c-myc, were obtained from the Protein Data Bank (PDB) with PDB IDs 2JSM,[68] 2KM3,[69] and 1XAV,[70] respectively. For CTA-22 and Tel-23, two K^+ atoms were added between the tetrads. Each structure was solvated with a truncated octahedron TIP4P-Ew water box,[71] as suggested in a recent work conducted on a G-quadruplex system.[72] The parm-BSC1 force field was used for the G4 structures.[73] Then, the solvated system was electrically neutralized with 0.10 M KCl and subjected to two minimization cycles of 5000 steps each: 2500 steps using steepest descent and other 2500 steps using conjugate gradient.[74] In the first cycle, we restrained the G4 heavy atoms with a 10 kcal mol^{-1} $Å^{-2}$ harmonic potential. Finally, the entire system was minimized without constraints. A 1 ns-long heating to 300 K in an NVT ensemble followed, restraining the movement of the G4 heavy atoms with a 10 kcal mol^{-1} $Å^{-2}$ harmonic potential. In order to ensure a slow release of the restraints, we performed three different 2 ns-long NPT equilibration runs by gradually decreasing the restraints to 1 kcal mol^{-1} $Å^{-2}$. In the first run, constraints were applied to the heavy atoms, whereas in the remaining two only to the G4 backbone. The production run was carried out without any restraint for 1.5 µs in the NPT ensemble. All simulations were performed applying the particle mesh Ewald (PME) truncation method (with a short-range cut-off of 10 Å), an integration step of 2 fs, the SHAKE algorithm, a Langevin thermostat with a friction coefficient of 1 ps^{-1}, the Monte Carlo thermostat for NPT simulations. All molecular dynamics simulations were run with AMBER18.

Molecular docking. Since we did not know "a priori" the binding site, we have performed blind docking with the AutoDock v4.2.2 program suite.[75] In particular, a search grid was centred on the Cartesian coordinates of the centre of mass of the G4 structure and defined by a box large enough to include the whole receptor macromolecule (120x120x120 points in x, y, and z directions with a spacing of 0.375 Å). The ligand molecules were treated as flexible during docking to allow for structural changes, while the G4 target was kept frozen in its original conformation throughout the docking procedure. The search was carried out with a Lamarckian genetic algorithm: a total of 200 docking runs for each target-ligand complex were carried out with a maximum of 25000000 energy evaluations. All other parameters were set to default values.

Conclusions

A new biscarbene complex of Ag(I) has been synthesised and characterised. Some tests on the Au(I) counterpart were done and evidenced the role of the metal centre. The higher cytotoxic activity compared to cisplatin can possibly be correlated to the cellular uptake and lipophilicity of the metal complexes. On the other hand, differences in the cytotoxicity between the two complexes are not correlated to the cellular uptake, indicating the importance of a different mode of action depending on the metal centre. Both $[Ag(BIA)_2]^+$ and $[Au(BIA)_2]^+$ can overcome the cisplatin resistance of ovarian cancer cells but the silver complex showed better results with a lower resistant factor and higher selectivity for cancer cells.
$[Ag(BIA)_2]^+$ showed high values of equilibrium constants (higher affinity with respect to gold) for the protein and the non-canonical structures of DNA (see Table S11), the latter being possible targets for this drug. Interestingly, a non-common and strong binding towards an i-motif is here shown for Ag(I)-NHCs. The same occurs for all parallel (c-myc), anti-parallel (CTA-22) and hybrid (Tel-23) G4 topologies, with different features. The dramatic changes of the anthracene spectroscopic profiles upon oligonucleotides binding tell us that these moieties are strongly involved in the reaction. This is true for both G4s and the i-motif. No similar discussion is possible for the wavelengths correlated to the ligand-metal coordination, as they overlap too much with the DNA absorbance range.[76]
The computational data on G4s agree with the experimental ones. Stacking interaction with the thymine residue on the loops was found to be the preferred binding mode for c-myc (the lower found value out of the three G4s), while for Tel-23, groove binding was the most stable pose. For CTA-22, an intermediate situation was found, in accordance with the melting data. As a matter of fact, the binding energies found for these metal-G4 complexes are estimated; molecular dynamics simulations would be necessary to better describe the ligand-receptor interactions.

Provided that the results are different for the different biosubstrates and considering the output of the theoretical calculations, the anthracenes seem to play a major role by interacting with the loops and the grooves of the oligos. Indeed, simple stacking over the G-tetrads or C-dyads would likely be much less tunable .[77] This seems a case where, oppositely, the compatibility between geometrical constraints for both metal complex and oligo grooves/loops plays a major role.[78] In this frame, note that the metal centre and the presence of two anthracenes will be fundamental to drive some peculiar geometrical arrangement.

The few experiments on $[Au(BIA)_2]^+$ showed an interaction with double strand DNA of poor interest since aggregation on DNA may be the major binding mode. Only FRET experiments gave positive results where a strong interaction with mitochondrial G4 (Fmt9438T) was found. Computational data demonstrated a slightly different geometry compared to the silver analogue and emerged a different preferential binding mode with c-myc. As a gold compound, the affinity for cysteine residues of the proteins is preserved, showing the formation of a kinetic adduct at short incubation times, with two gold complexes in a Au---S---Au coordination geometry, with the loss of one of the two carbene ligands.

It is worth noting that the complexes studied in our previous work,[26] with an ethyl carbon chain on the imidazole, instead of a butyl one, demonstrated a different behaviour from two different points of view. First, the silver biscarbene could not bind the G4 structure, validating our hypothesis that a longer carbon chain could enhance the affinity for this non-canonical DNA structure. Secondly, the binding with the serum albumin could not give a covalent binding with the protein, and the driving force of the whole interaction was found to be based on electrostatics (connected to lower hydrophobicity) while, in this study, the silver biscarbene covalently binds the Cys34 residue with the loss of one carbene ligand.

Notably, this is the first example of a silver carbene which can bind G4s and i-motif structures. This can put into play new mechanisms of action that can improve the efficiency of the anticancer drug.

Author Contributions

Conceptualisation: F.B., E.G., G.S., A.P., T.B.; data curation: F.B., E.G., G.S. and D.C.; formal analysis: F.B, E.G., G.S., D.C., M.S., A.D. and L.G.; funding acquisition: F.B, E.G., G.S., A.P. and T.B.; investigation: F.B, E.G., G.S., D.C., M.S., A.D. and L.G.; methodology: D.C., N.B., B.G., A.P and T.B.; supervision: D.C., N.B., B.G., A.P. and T.B.; writing – original draft: F.B., E.G. and G.S.; writing – review and editing: all authors.

† These authors contributed equally.

* Corresponding authors:
F. Binacchi (francesca.binacchi@dcci.unipi.it),
E. Giorgi (ester.giorgi@phd.unipi.it),
G. Salvadori (giacomo.salvadori@phd.unipi.it).

Conflicts of interest

There are no conflicts to declare.

Acknowledgements

FB, EG and GS thank the DSCM and DCCI of the University of Pisa for financial support with the interdisciplinary project PRIMULE (PRomoting Innovative and MULtidisciplinary Experiments at DSCM). This contribution is part of the work from COST Action CA18202, NECTAR Network for Equilibria and Chemical Thermodynamics Advanced Research, supported by COST (European Cooperation in Science and Technology). AP gratefully acknowledges funding by the University of Pisa under the "PRA–Progetti di Ricerca di Ateneo" (Institutional Research Grants), project no. PRA_2022-2023_12 "New challenges of transition metal and lanthanide complexes in the perspective of green chemistry".

Notes and references

1 M. N. Hopkinson, C. Richter, M. Schedler and F. Glorius, *Nature*, 2014, **510**, 485–496.
2 J. C. Garrison and W. J. Youngs, *Chem. Rev.*, 2005, **105**, 3978–4008.
3 A. Citta, E. Schuh, F. Mohr, A. Folda, M. L. Massimino, A. Bindoli, A. Casini and M. P. Rigobello, *Metallomics*, 2013, **5**, 1006.
4 W. Streciwilk, A. Terenzi, F. Lo Nardo, P. Prochnow, J. E. Bandow, B. K. Keppler and I. Ott, *Eur J Inorg Chem*, 2018, **2018**, 3104–3112.
5 C. K. Mirabelli, R. K. Johnson, M. Sung, L. Faucette, K. Muirhead and S. T. Crooke, *Cancer Res*, 1985, **45**, 32–39.
6 Available at, https://classic.clinicaltrials.gov/ct2/results?term=auranofin&Search=Apply&age_v=&gndr=&type=&rslt=.
7 M. Kupiec, R. Ziółkowski, L. Massai, L. Messori and K. Pawlak, *J. of Inorg. Biochem.*, 2019, **198**, 110714.
8 J. H. Kim, E. Reeder, S. Parkin and S. G. Awuah, *Sci Rep*, 2019, **9**, 12335.
9 M. P. Sullivan, H. U. Holtkamp and C. G. Hartinger, in *Metallo-Drugs: Development and Action of Anticancer Agents*, eds. A. Sigel, H. Sigel, E. Freisinger and R. K. O. Sigel, De Gruyter, 2018, pp. 351–386.
10 M. Mora, M. C. Gimeno and R. Visbal, *Chem. Soc. Rev.*, 2019, **48**, 447–462.
11 S. K. Raju, S. K, P. S, M. M and M. K, *GJPB*, 2022, **1**, 06–28.
12 S. B. Aher, P. N. Muskawar, K. Thenmozhi and P. R. Bhagat, *European Journal of Medicinal Chemistry*, 2014, **81**, 408–419.
13 N. Pandya, S. R. Bhagwat and A. Kumar, *Biochimica et Biophysica Acta (BBA) - Reviews on Cancer*, 2021, **1876**, 188594.
14 V. Bernat and M. D. Disney, *Neuron*, 2015, **87**, 28–46.
15 B. Bertrand, L. Stefan, M. Pirrotta, D. Monchaud, E. Bodio, P. Richard, P. Le Gendre, E. Warmerdam, M. H. de Jager, G. M. M. Groothuis, M. Picquet and A. Casini, *Inorg. Chem.*, 2014, **53**, 2296–2303.
16 S. Gama, I. Rodrigues, F. Mendes, I. C. Santos, E. Gabano, B. Klejevskaja, J. Gonzalez-Garcia, M. Ravera, R. Vilar and A. Paulo, *Journal of Inorganic Biochemistry*, 2016, **160**, 275–286.

17 C. Nakanishi and H. Seimiya, *Biochemical and Biophysical Research Communications*, 2020, **531**, 45–50.
18 T. Kench and R. Vilar, in *Annual Reports in Medicinal Chemistry*, Elsevier, 2020, vol. 54, pp. 485–515.
19 S. M. Meier-Menches, B. Neuditschko, K. Zappe, M. Schaier, M. C. Gerner, K. G. Schmetterer, G. Del Favero, R. Bonsignore, M. Cichna-Markl, G. Koellensperger, A. Casini and C. Gerner, *Chem. Eur. J.*, 2020, **26**, 15528–15537.
20 L. Martino, B. Pagano, I. Fotticchia, S. Neidle and C. Giancola, *J. Phys. Chem. B*, 2009, **113**, 14779–14786.
21 P. Alberti, J. Ren, M. P. Teulade-Fichou, L. Guittat, J.-F. Riou, J. B. Chaires, C. Hélène, J.-P. Vigneron, J.-M. Lehn and J.-L. Mergny, *Journal of Biomolecular Structure and Dynamics*, 2001, **19**, 505–513.
22 S. Shi, X. Geng, J. Zhao, T. Yao, C. Wang, D. Yang, L. Zheng and L. Ji, *Biochimie*, 2010, **92**, 370–377.
23 S. Shi, J. Zhao, X. Geng, T. Yao, H. Huang, T. Liu, L. Zheng, Z. Li, D. Yang and L. Ji, *Dalton Trans.*, 2010, **39**, 2490.
24 H. Xu, H. Zhang and X. Qu, *Journal of Inorganic Biochemistry*, 2006, **100**, 1646–1652.
25 A. S. Tikhomirov, M. A. S. Abdelhamid, G. Y. Nadysev, G. V. Zatonsky, E. E. Bykov, P. J. Chueh, Z. A. E. Waller and A. E. Shchekotikhin, *J. Nat. Prod.*, 2021, **84**, 1617–1625.
26 F. Binacchi, F. Guarra, D. Cirri, T. Marzo, A. Pratesi, L. Messori, C. Gabbiani and T. Biver, *Molecules*, 2020, **25**, 5446.
27 M. G. Fabbrini, D. Cirri, A. Pratesi, L. Ciofi, T. Marzo, A. Guerri, S. Nistri, A. Dell'Accio, T. Gamberi, M. Severi, A. Bencini and L. Messori, *ChemMedChem*, 2019, **14**, 182–188.
28 F. Macii and T. Biver, *J. of Inorg. Biochem.*, 2021, **216**, 111305.
29 M. H. Rahman, T. Maruyama, T. Okada, K. Yamasaki and M. Otagiri, *Biochem. Pharm.*, 1993, **46**, 1721–1731.
30 S. Awasthi and N. T. Saraswathi, *RSC Adv.*, 2016, **6**, 90739–90753.
31 I. Rombouts, B. Lagrain, K. A. Scherf, M. A. Lambrecht, P. Koehler and J. A. Delcour, *Sci Rep*, 2015, **5**, 12210.
32 S. Sen, M. W. Perrin, A. C. Sedgwick, V. M. Lynch, J. L. Sessler and J. F. Arambula, *Chem. Sci.*, 2021, **12**, 7547–7553.
33 A. A. Isab, C. F. Shaw, J. D. Hoeschele and J. Locke, *Inorg. Chem.*, 1988, **27**, 3588–3592.
34 M. T. Coffer, C. F. Shaw, M. K. Eidsness, J. W. Watkins and R. C. Elder, *Inorg. Chem.*, 1986, **25**, 333–339.
35 A. Pratesi, D. Cirri, L. Ciofi and L. Messori, *Inorg. Chem.*, 2018, **57**, 10507–10510.
36 A. Pratesi, D. Cirri, D. Fregona, G. Ferraro, A. Giorgio, A. Merlino and L. Messori, *Inorg. Chem.*, 2019, **58**, 10616–10619.
37 C. Zoppi, L. Massai, D. Cirri, C. Gabbiani, A. Pratesi and L. Messori, *Inorganica Chimica Acta*, 2021, **520**, 120297.
38 D. Cirri, L. Massai, C. Giacomelli, M. L. Trincavelli, A. Guerri, C. Gabbiani, L. Messori and A. Pratesi, *Dalton Trans.*, 2022, **51**, 13527–13539.
39 A. Giorgio and A. Merlino, *Coordination Chemistry Reviews*, 2020, **407**, 213175.
40 J. Xiao and C. F. Shaw, *Inorg. Chem.*, 1992, **31**, 3706–3710.
41 C. Bazzicalupi, A. Bencini, A. Bianchi, T. Biver, A. Boggioni, S. Bonacchi, A. Danesi, C. Giorgi, P. Gratteri, A. M. Ingraín, F. Secco, C. Sissi, B. Valtancoli and M. Venturini, *Chemistry A European J*, 2008, **14**, 184–196.
42 G. Scatchard, *Annals of the New York Academy of Sciences*, 1949, **51**, 660–672.
43 H. A. Benesi and J. H. Hildebrand, *J. Am. Chem. Soc.*, 1949, **71**, 2703–2707.
44 J. D. McGhee and P. H. Von Hippel, *Journal of Molecular Biology*, 1974, **86**, 469–489.
45 N. Busto, J. Valladolid, C. Aliende, F. A. Jalón, B. R. Manzano, A. M. Rodríguez, J. F. Gaspar, C. Martins, T. Biver, G. Espino, J. M. Leal and B. García, *Chem. Asian J.*, 2012, **7**, 788–801.
46 T. Biver, F. Secco, M. R. Tinè, M. Venturini, A. Bencini, A. Bianchi and C. Giorgi, *Journal of Inorganic Biochemistry*, 2004, **98**, 1531–1538.
47 B. K. Paul and N. Guchhait, *J. Phys. Chem. B*, 2011, **115**, 11938–11949.
48 S. Ramakrishnan and M. Palaniandavar, *J Chem Sci*, 2005, **117**, 179–186.
49 L. Wang, G. Zhang, J. Pan, C. Xiong and D. Gong, *J. of Photochem. and Photobio. B: Bio.*, 2014, **141**, 253–261.
50 A. R. Rubio, R. González, N. Busto, M. Vaquero, A. L. Iglesias, F. A. Jalón, G. Espino, A. M. Rodríguez, B. García and B. R. Manzano, *Pharm.*, 2021, **13**, 1540.
51 J. Amato, G. Miglietta, R. Morigi, N. Iaccarino, A. Locatelli, A. Leoni, E. Novellino, B. Pagano, G. Capranico and A. Randazzo, *J. Med. Chem.*, 2020, **63**, 3090–3103.
52 S. Mohammadi, Z. Narimani, M. Ashouri, R. Firouzi and M. H. Karimi-Jafari, *Sci Rep*, 2022, **12**, 410.
53 R. E. Amaro, J. Baudry, J. Chodera, Ö. Demir, J. A. McCammon, Y. Miao and J. C. Smith, *Biophysical Journal*, 2018, **114**, 2271–2278.
54 W. Evangelista Falcon, S. R. Ellingson, J. C. Smith and J. Baudry, *J. Phys. Chem. B*, 2019, **123**, 5189–5195.
55 P. Murat, Y. Singh and E. Defrancq, *Chem. Soc. Rev.*, 2011, **40**, 5293.
56 H. Mach, C. R. Middaugh and R. V. Lewis, *Anal. Biochem.*, 1992, **200**, 74–80.
57 G. Felsenfeld and S. Z. Hirschman, *J. of Molec. Bio.*, 1965, **13**, 407–427.
58 T. Biver, F. Secco and M. Venturini, *Arch. of Biochem. and Biophy.*, 2005, **437**, 215–223.
59 A. R. Rubio, N. Busto, J. M. Leal and B. García, *RSC Adv.*, 2016, **6**, 101142–101152.
60 X. Long and M. D. Stone, *PLoS ONE*, 2013, **8**, e83420.
61 D. Cirri, A. Geri, L. Massai, M. Mannelli, T. Gamberi, F. Magherini, M. Becatti, C. Gabbiani, A. Pratesi and L. Messori, *Molecules*, 2023, **28**, 1050.
62 A. Menconi, T. Marzo, L. Massai, A. Pratesi, M. Severi, G. Petroni, L. Antonuzzo, L. Messori, S. Pillozzi and D. Cirri, *Biometals*, 2021, **34**, 867–879.
63 G. Ciancaleoni, S. Rampino, D. Zuccaccia, F. Tarantelli, P. Belanzoni and L. Belpassi, *J. Chem. Theory Comput.*, 2014, **10**, 1021–1034.
64 Y. Minenkov, Å. Singstad, G. Occhipinti and V. R. Jensen, *Dalton Trans.*, 2012, **41**, 5526.
65 G. Scalmani and M. J. Frisch, *The Journal of Chemical Physics*, 2010, **132**, 114110.
66 E. Cancès, B. Mennucci and J. Tomasi, *The Journal of Chemical Physics*, 1997, **107**, 3032–3041.
67 J. Tomasi, B. Mennucci and R. Cammi, *Chem. Rev.*, 2005, **105**, 2999–3094.
68 A. T. Phan, V. Kuryavyi, K. N. Luu and D. J. Patel, *Nucleic Acids Research*, 2007, **35**, 6517–6525.
69 K. W. Lim, P. Alberti, A. Guédin, L. Lacroix, J.-F. Riou, N. J. Royle, J.-L. Mergny and A. T. Phan, *Nucleic Acids Research*, 2009, **37**, 6239–6248.
70 A. Ambrus, D. Chen, J. Dai, R. A. Jones and D. Yang, *Biochemistry*, 2005, **44**, 2048–2058.

71 H. W. Horn, W. C. Swope, J. W. Pitera, J. D. Madura, T. J. Dick, G. L. Hura and T. Head-Gordon, *The Journal of Chemical Physics*, 2004, **120**, 9665–9678.
72 M. Castelli, F. Doria, M. Freccero, G. Colombo and E. Moroni, *J. Chem. Theory Comput.*, 2022, **18**, 4515–4528.
73 I. Ivani, P. D. Dans, A. Noy, A. Pérez, I. Faustino, A. Hospital, J. Walther, P. Andrio, R. Goñi, A. Balaceanu, G. Portella, F. Battistini, J. L. Gelpí, C. González, M. Vendruscolo, C. A. Laughton, S. A. Harris, D. A. Case and M. Orozco, *Nat Methods*, 2016, **13**, 55–58.
74 J. D. Schmit, N. L. Kariyawasam, V. Needham and P. E. Smith, *J. Chem. Theory Comput.*, 2018, **14**, 1823–1827.
75 G. M. Morris, R. Huey, W. Lindstrom, M. F. Sanner, R. K. Belew, D. S. Goodsell and A. J. Olson, *J. Comput. Chem.*, 2009, **30**, 2785–2791.
76 L. Messori, L. Marchetti, L. Massai, F. Scaletti, A. Guerri, I. Landini, S. Nobili, G. Perrone, E. Mini, P. Leoni, M. Pasquali and C. Gabbiani, *Inorg. Chem.*, 2014, **53**, 2396–2403.
77 T. Santos, G. F. Salgado, E. J. Cabrita and C. Cruz, *Pharmaceuticals*, 2021, **14**, 769.
78 A. Arora and S. Maiti, *J. Phys. Chem. B*, 2008, **112**, 8151–8159.